

High-Statistics Measurement of Neutrino Quasielasticlike Scattering at 6 GeV on a Hydrocarbon Target

M. F. Carneiro,^{1,2,*} D. Ruterbories,³ Z. Ahmad Dar,⁴ F. Akbar,⁴ D. A. Andrade,⁵ M. V. Ascencio,⁶ W. Badgett,⁷ A. Bashyal,¹ A. Bercellie,³ M. Betancourt,⁷ K. Bonin,⁸ A. Bravar,⁹ H. Budd,³ G. Caceres,² T. Cai,³ H. da Motta,² G. A. Díaz,^{3,6} J. Felix,⁵ L. Fields,⁷ A. Filkins,¹⁰ R. Fine,³ A. M. Gago,⁶ A. Ghosh,^{11,2} R. Gran,⁸ D. Hahn,⁷ D. A. Harris,^{12,7} S. Henry,³ J. Hylen,⁷ S. Jena,¹³ D. Jena,⁷ C. Joe,⁷ B. King,⁷ J. Kleykamp,³ M. Kordosky,¹⁰ D. Last,¹⁴ T. Le,^{15,16} J. LeClerc,¹⁷ A. Lozano,² X.-G. Lu,¹⁸ E. Maher,¹⁹ S. Manly,³ W. A. Mann,¹⁵ K. S. McFarland,³ C. L. McGivern,^{7,20} A. M. McGowan,³ B. Messerly,²⁰ J. Miller,¹¹ J. G. Morfín,⁷ M. Murphy,⁷ D. Naples,²⁰ J. K. Nelson,¹⁰ C. Nguyen,¹⁷ A. Norrick,¹⁰ A. Olivier,³ V. Paolone,²⁰ G. N. Perdue,^{7,3} P. Riehecky,⁷ H. Schellman,¹ P. Schlabach,⁷ C. J. Solano Salinas,²¹ H. Su,²⁰ M. Sultana,³ V. S. Syrotenko,¹⁵ D. Torretta,⁷ C. Wret,³ B. Yaeggy,¹¹ K. Yonehara,⁷ and L. Zazueta¹⁰

¹Department of Physics, Oregon State University, Corvallis, Oregon 97331, USA

²Centro Brasileiro de Pesquisas Físicas, Rua Doutor Xavier Sigaud 150, Urca, Rio de Janeiro, Rio de Janeiro, 22290-180, Brazil

³Department of Physics and Astronomy, University of Rochester, Rochester, New York 14627, USA

⁴AMU Campus, Aligarh, Uttar Pradesh 202001, India

⁵Campus León y Campus Guanajuato, Universidad de Guanajuato, Lascurain de Retana 5, Colonia Centro, Guanajuato 36000, Mexico

⁶Sección Física, Departamento de Ciencias, Pontificia Universidad Católica del Perú, Apartado 1761, Lima, Perú

⁷Fermi National Accelerator Laboratory, Batavia, Illinois 60510, USA

⁸Department of Physics, University of Minnesota Duluth, Duluth, Minnesota 55812, USA

⁹Département de Physique Nucléaire et Corpusculaire, University of Geneva, 1211 Geneva 4, Switzerland

¹⁰Department of Physics, College of William & Mary, Williamsburg, Virginia 23187, USA

¹¹Departamento de Física, Universidad Técnica Federico Santa María, Avenida España 1680 Casilla 110-V, Valparaíso, Chile

¹²Department of Physics and Astronomy, Toronto, Ontario, M3J 1P3 Canada

¹³Department of Physical Sciences, IISER Mohali, Knowledge City, SAS Nagar, Mohali 140306, Punjab, India

¹⁴Department of Physics and Astronomy, University of Pennsylvania, Philadelphia, Pennsylvania 19104, USA

¹⁵Physics Department, Tufts University, Medford, Massachusetts 02155, USA

¹⁶Rutgers, The State University of New Jersey, Piscataway, New Jersey 08854, USA

¹⁷University of Florida, Department of Physics, Gainesville, Florida 32611, USA

¹⁸Oxford University, Department of Physics, Oxford OX1 3PJ, United Kingdom

¹⁹Department of Physics, Massachusetts College of Liberal Arts, 375 Church Street, North Adams, Massachusetts 01247, USA

²⁰Department of Physics and Astronomy, University of Pittsburgh, Pittsburgh, Pennsylvania 15260, USA

²¹Facultad de Ciencias, Universidad Nacional de Ingeniería, Apartado 31139, Lima, Perú



(Received 20 December 2019; revised manuscript received 1 February 2020; accepted 5 February 2020; published 24 March 2020)

We measure neutrino charged-current quasielasticlike scattering on hydrocarbon at high statistics using the wideband Neutrinos at the Main Injector beam with neutrino energy peaked at 6 GeV. The double-differential cross section is reported in terms of muon longitudinal (p_{\parallel}) and transverse (p_{\perp}) momentum. Cross section contours versus lepton momentum components are approximately described by a conventional generator-based simulation, however, discrepancies are observed for transverse momenta above 0.5 GeV/ c for longitudinal momentum ranges 3–5 and 9–20 GeV/ c . The single differential cross section versus momentum transfer squared ($d\sigma/dQ_{QE}^2$) is measured over a four-decade range of Q^2 that extends to 10 GeV². The cross section turnover and falloff in the Q^2 range 0.3–10 GeV² is not fully reproduced by generator predictions that rely on dipole form factors. Our measurement probes the axial-vector content of the hadronic current and complements the electromagnetic form factor data obtained using electron-nucleon elastic scattering. These results help oscillation experiments because they probe the importance of various correlations and final-state interaction effects within the nucleus, which have different effects on the visible energy in detectors.

DOI: 10.1103/PhysRevLett.124.121801

Published by the American Physical Society under the terms of the [Creative Commons Attribution 4.0 International license](https://creativecommons.org/licenses/by/4.0/). Further distribution of this work must maintain attribution to the author(s) and the published article's title, journal citation, and DOI. Funded by SCOAP³.

The charged-current quasielastic (CCQE) neutrino interaction (i.e., $\nu_\mu n \rightarrow \mu^- p$) is an important channel in the E_ν range of a few GeV and is of value in searches for leptonic CP -symmetry violation [1–6]. Because there is little missing energy, this channel allows a good estimate of the incident neutrino energy. However, imperfect knowledge of nuclear effects remains a limiting factor for oscillation measurements [7]. These uncertainties are significant in current experiments [1–4] and will become more important with the statistics of DUNE [5] and Hyper-Kamiokande [6].

For free nucleons, quasielastic scattering is described by the standard theory of weak interactions combined with nucleon form factors [8]. Electron-nucleon scattering experiments [9] measure the electromagnetic form factors, but measurement of the axial-vector form factor F_A , at four-momentum transfer squared $Q^2 \sim 0.1 \text{ GeV}^2$, can only be done via $\nu/\bar{\nu}$ nucleon scattering.

The axial-vector form factor is usually parametrized using the dipole form and has been measured at zero energy transfer through beta-decay experiments [10,11]. The vector (V), axial-vector (A), and VA interference terms of free-nucleon hadronic currents have been studied on free or quasifree nucleons on hydrogen and deuterium targets [12–15].

Neutrino oscillation experiments in the few-GeV range, however, use detectors constructed of carbon [3,16], oxygen [17], iron [18], or argon [5,19]. Nuclear effects are significant and must be modeled for these experiments to reach their full physics potential. Historically, a relativistic Fermi gas (RFG) [20] has been used to model the initial-state nucleon, but modifications are necessary to reproduce experimental data [3,16,21,22]. The local Fermi gas (LFG) is an extension to the RFG with a local density approximation [23,24]. Alternatively, spectral function (SF) techniques [25] use a mean field to replace the sum of individual interactions.

Long-range correlations between nucleons are modeled using a random-phase approximation (RPA) correction [26–31] to account for the screening effect that arises from the proximity of other nucleons in the nuclear potential well. The RPA correction reduces the interaction rate at low Q^2 while enhancing moderate Q^2 interactions.

A wide range of two-particle, two-hole models using a meson-exchange formalism are tested against electron scattering (e, e) data [32–38]. Attempts to predict the neutrino rate and pp and pn knockout rate are given in [27,39–41]. This analysis uses a simulation with the Valencia $2p2h$ model [39].

A complete description of the experimental signature for quasielastic scattering must also account for the propagation through the nucleus of particles produced by any initial charged-current interaction. The charged lepton produced escapes the nucleus without interacting but final-state hadrons are likely to interact. Such final-state interactions

(FSI) may produce new particles such as pions or mimic the CCQE signal through absorption of pions in resonance production. In both cases, the observed final state differs from the original interaction.

We use a topology-based signal definition where a muon, zero or more nucleons, and no mesons or heavy baryons are in the final state (CCQE-like). CCQE-like processes include pion production, where the pion is absorbed in the nucleus and $2p2h$ processes where more than one nucleon is produced. The history of CCQE measurements is extensive [21,22,42–54], but the community has yet to converge on a full description of the nuclear effects since the measured final state is determined by a mixture of initial interaction dynamics and nuclear effects.

In this Letter, we report a study of muon neutrino CCQE-like interactions in the Neutrinos at Main Injector (NuMI) [55] “medium energy” beam. The data correspond to an exposure of 1.061×10^{21} protons on target (POT), which combined with the higher flux per POT results in over a factor of 10 increase in statistics above our previous measurements [21,45,52,54]. The new configuration provides a broad neutrino flux peaked at 6 GeV. We present two-dimensional cross sections for CCQE-like scattering as a function of muon transverse (p_\perp) and longitudinal (p_\parallel) momentum. We also report the differential cross section versus the square of the momentum transferred using a quasielastic interaction hypothesis, where $Q_{QE}^2 = 2E_\nu(E_\mu - p_\parallel) - M_\mu^2$ and the neutrino energy E_ν is also determined using the quasielastic (QE) hypothesis (see [54]). This result extends the Q_{QE}^2 range by a factor of 4 compared to previous measurements.

The NuMI beam line consists of a 120-GeV primary proton beam, a two-interaction-length graphite target, two parabolic focusing horns, and a 675-m decay pipe. For these data, taken between 2013 and 2017, the horn polarities are set to create a neutrino-dominated beam. The beam line is modeled with a Geant4-based [56,57] simulation (g4numi [58] version 6, built against Geant version v.9.4.p2). There are known discrepancies between Geant4 predictions of proton on carbon and other interactions relevant to NuMI flux predictions. MINERVA corrects the Geant4 flux predictions with hadron-production data [58]. In addition, measurements of neutrino-electron ($\nu - e$) scatters, as described in [59], constrain the flux and reduces the normalization uncertainty on the integrated flux between 2 and 20 GeV from 7.8% to 3.9%.

We restrict this study to events originating in the central scintillator tracker region of the MINERVA detector [60]. The target mass consists of 88.5%, 8.2%, and 2.5% carbon, hydrogen, and oxygen, respectively, plus small amounts of heavier nuclei. The 5.3-ton tracker fiducial region is followed by an electromagnetic calorimeter made up of 20 scintillator planes interleaved with 0.2-cm thick lead sheets, followed by a hadronic calorimeter region of 20 scintillator planes interleaved with 2.54-cm thick iron slabs.

The magnetized MINOS muon spectrometer [61] begins 2 m downstream and provides momentum and charge information for muons.

Neutrino interactions are simulated using the GENIE 2.12.6 event generator [62]. The GENIE default interaction model is adjusted to match MINERvA GENIE tune v1 (MnvGENIEv1). This model includes three modifications to the default GENIE model. First, the Valencia RPA correction [26,63], appropriate for a Fermi gas [27,31], is added as a function of energy and three-momentum transfer. Second, the prediction for multinucleon scattering given by the Valencia model [64–66] in GENIE 2.12.6 is added and modified with an empirical fit [67] based on previous MINERvA data. The modification, referred to as the “low-recoil fit,” increases the integrated $2p2h$ rate by 49%. Finally, nonresonant pion production is reduced by 57% to agree with a fit to measurements of that process on deuterium [68].

The kinematics of each interaction are reconstructed using the measured muon momentum and angle with respect to the beam as described in [54]. To address the MINOS acceptance, only events with muons created within $< 20^\circ$ of the neutrino beam and above $1.5 \text{ GeV}/c$ in momentum are accepted.

As a cross-check of its flux predictions, MINERvA also uses samples of neutrino-nucleus interactions with less than 800 MeV transferred to the hadronic system. Data and simulation comparisons show a discrepancy as a function of neutrino energy. To determine the source of this discrepancy, we fit the neutrino energy distributions in different spatial regions of the detector to templates that allow both the beam line parameters (i.e., focusing horn current and position) and the muon energy scale to float. Hadron-production and neutrino interaction uncertainties are evaluated to obtain the systematic uncertainty on the fit results. The data and simulation prediction before and after the muon energy scale shift are shown in the Supplemental Material [69]. The discrepancy is most consistent with a 3.6% muon energy scale shift, which is 1.8 times the *a priori* energy scale uncertainty. In this analysis, the reconstructed muon energy is shifted by 3.6%, with an uncertainty of 1.0% (the posterior uncertainty from the fit).

We retain two populations of events: a muon-only sample with no identified proton and a muon + proton sample. These samples are analyzed separately since their background components have different sources. For both of these populations, there are three sidebands used to constrain three backgrounds, as described in [54].

As the signal definition for CCQE-like interactions includes no final-state mesons or heavy baryons, the energy loss profiles of tracks contained within MINERvA are required to be consistent with a proton hypothesis. For events with $Q_{QE}^2 > 0.6 \text{ GeV}^2$ the proton-interaction probability is high, so no energy loss cut is made in this region. This results in a small discontinuity in the transverse momentum distributions for the muon + additional track

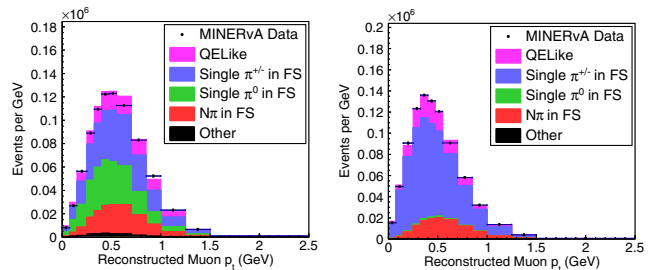


FIG. 1. One-track sideband p_T distributions for data and predictions after fitting, for (left) π^0 and (right) π^\pm Michel candidates.

samples. To reduce inelastic backgrounds, events with untracked energy above 0.5 GeV are removed. Events with Michel electrons (from the decay chain $\pi^\pm \rightarrow \mu^\pm \rightarrow e^\pm$) are also vetoed.

The first sideband consists of events having two or more clusters of energy detached from the primary vertex, but passing all other cuts. This sample, shown in Fig. 1 (left), helps constrain backgrounds from processes with π^0 's in the final state (FS) or events where a π^+ charge exchanges. The second sideband consists of events passing all cuts but the Michel electron cut. This sample is primarily sensitive to backgrounds from charged pions, as shown in Fig. 1 (right). The third (and smallest) sideband comes from events with both a Michel electron and extra clusters, and it is sensitive to multipion events.

To constrain the background predictions, simultaneous fits are made to the three sidebands as a function of muon transverse momentum, for the single- and multitrack topologies separately. Templates based on three simulated background distributions are fit to the data and the resulting three background normalizations for each topology are used to estimate the contamination from each source. The effect of the fit on the backgrounds versus muon transverse momentum is shown in the Supplemental Material [69]. Using the fit results, we subtract the predicted backgrounds from the data in each bin. The one- and multitrack signal samples have 670 022 and 648 518 events, respectively,

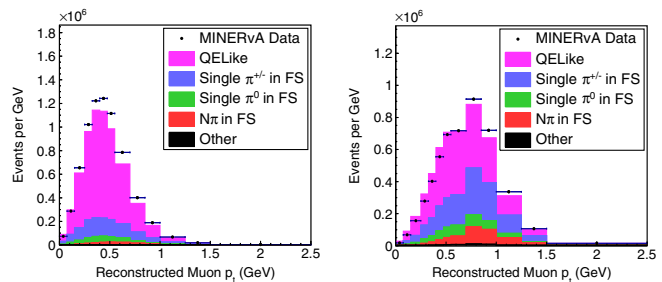


FIG. 2. Reconstructed muon transverse momentum in (left) one-track and (right) two + track signal samples. The primary background in both samples comes from charged-current pion production.

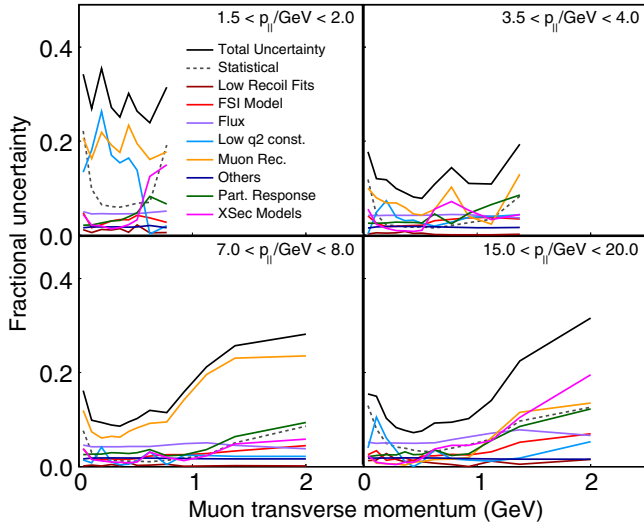


FIG. 3. Fractional systematic uncertainty on the double-differential cross section as a function of p_{\perp} and p_{\parallel} .

and are shown in Fig. 2 with the predicted backgrounds after the fit.

After background subtraction, the data are unfolded, following the method of D’Agostini [70,71], via the implementation in RooUnfold [72] using four iterations. To minimize model dependence, the unfolded Q_{QE}^2 is the one calculated with the true muon kinematics assuming a quasielastic hypothesis, not the generator-level momentum transfer squared. The unfolded sample is corrected for

selection efficiency as predicted by the simulation. The selection has an average efficiency of 70% in bins inside the edges of the phase space. The efficiency is approximately 70% below 0.1 GeV^2 in Q_{QE}^2 , reducing to 10% at 10 GeV^2 . The efficiency-corrected distributions are normalized by the integral of the predicted neutrino flux in the 0–120 GeV range and by the number of nucleons (3.23×10^{30} in the fiducial region) to derive differential cross sections.

The cross section uncertainties for four representative p_{\parallel} bins are shown in Fig. 3. Uncertainties for remaining bins and for the Q_{QE}^2 result are available in the Supplemental Material [69]. Muon reconstruction uncertainties, which include muon energy scale, resolution, and angle uncertainties, dominate in most bins. A description of the remaining uncertainty classes and how they are assessed can be found in [54]. Additionally, we add an uncertainty to account for the possibility of low- Q^2 suppression in pion events, evaluated by adding the low- Q^2 suppression described in [73] to our default model. The flux uncertainties are described in [59].

The double-differential cross section is presented in Fig. 4. Here, $M_{\text{nuGENIEv1}}$ serves as a reference simulation to which the data are compared. The simulation is seen to reproduce the data at zeroth order, but discrepancies are apparent. Bins above the spectral peak in p_T are underpredicted in the p_{\parallel} range 3.0–5.0 GeV. From 5.5 to 8.0 GeV, the distributions below the spectral peak are overpredicted; underprediction of event rate resumes

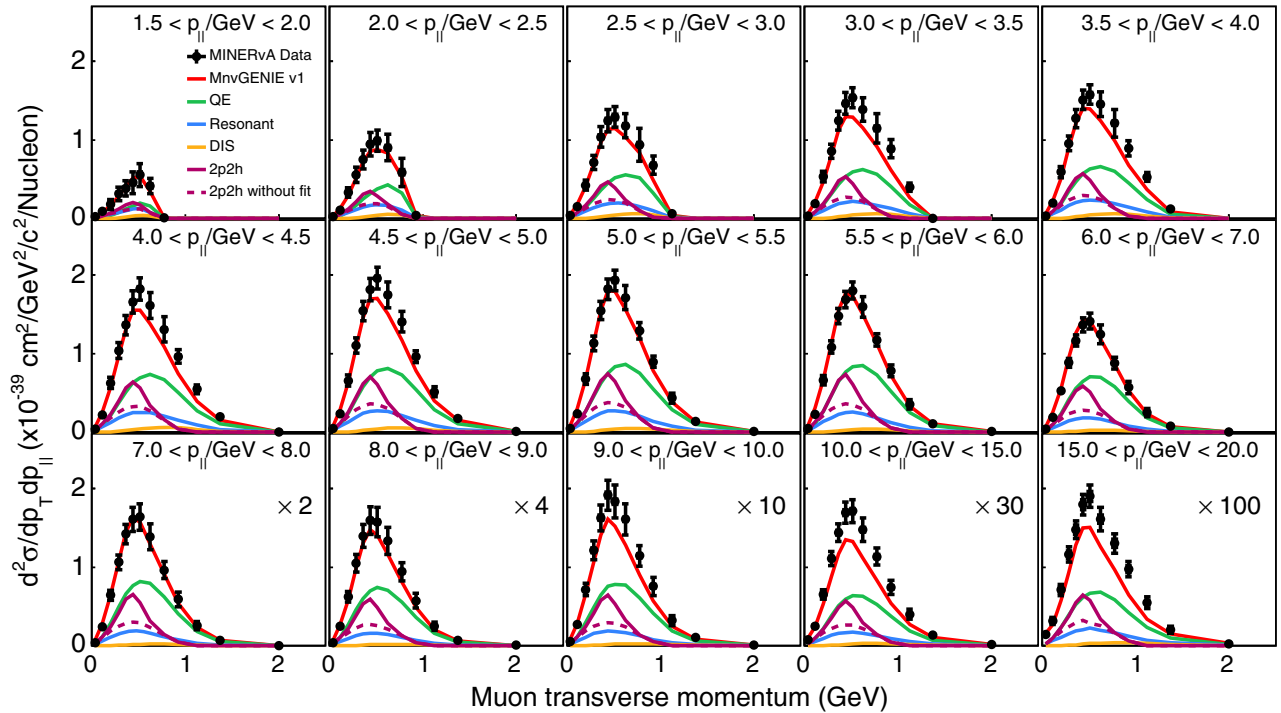


FIG. 4. $d^2\sigma/dp_{\perp}/dp_{\parallel}$ for data and the $M_{\text{nuGENIEv1}}$ reference simulation in bins of p_{\parallel} . The predictions for the contributions to the final-state signal channel from CCQE, resonant, deep-inelastic scattering (DIS), and $2p2h$ processes are also shown.

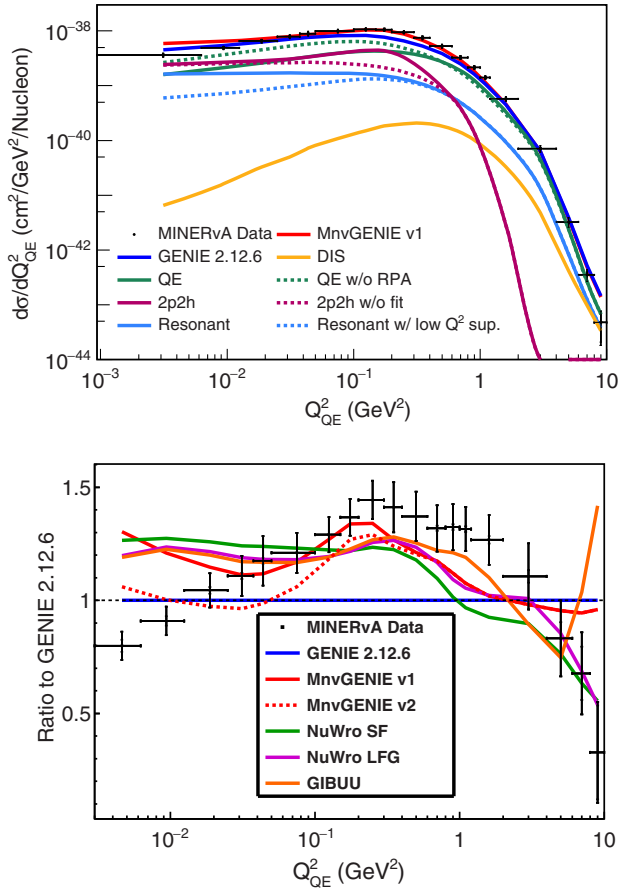


FIG. 5. Top: Differential cross section as a function of Q^2 . Bottom: Generator predictions compared to data. All are plotted as ratio to the predictions of unmodified GENIE 2.12.6.

dramatically at p_{\parallel} above 9.0 GeV. The simulation shows that CCQE and $2p2h$ comprise the dominant spectral components and that discrepancies could be alleviated by modest adjustments, particularly for CCQE at higher p_T .

The single-differential cross section $d\sigma/dQ_{QE}^2$ is presented in Fig. 5 (top). The falloff of the cross section for $Q^2 > 1.0$ GeV² is reproduced at moderate and high Q^2 by the MnvGENIEv1 reference simulation, indicating that dipole forms for the vector and axial-vector nucleon form factors remain appropriate. Figure 5 (bottom) shows the ratio of data and selected generators to the reference simulation. Here the cross section turnover in the range from 0.3 to ~ 3.0 GeV² proceeds more gradually than predicted; all generators underpredict the data throughout this region. These general features are similar to those observed for the electromagnetic form factors in electron-nucleon elastic scattering experiments (see Fig. 17 of [74]). The present Letter, by mapping neutrino quasielastic scattering into the multi-GeV Q^2 region, provides new information about the axial-vector part of the nucleon current that cannot be

TABLE I. χ^2 of model variants derived from the GENIE, NuWro and GiBUU event generators compared to $[(d^2\sigma)/(dp_{\perp}dp_{\parallel})]$. Both standard and log-normal χ^2 are shown; the number of degrees of freedom for each comparison is 184.

Model	χ^2 - linear	χ^2 - log
GENIE 2.12.6	1031	1543
+ π tune	1071	1669
+RPA + π tune	420	927
+RPA + π tune + MINOS low Q^2 sup.	403	986
GENIE 2.12.6 + 2p2h	2299	1913
+RPA + π tune + recoil fit (MnvGENIEv1)	1194	1155
+ π tune	2377	2039
+RPA + π tune	1068	1221
+recoil fit + RPA + π tune + MINOS low Q^2 sup.	870	989
+recoil fit + RPA + π tune + Nieves low Q^2 sup.	921	1000
+recoil fit + π tune	2714	2052
+recoil fit + RPA + π tune + MINERvA low Q^2 sup.	799	953
GiBUU	1729	1890
NuWro SF	3533	6188
NuWro LFG	3176	5914
GENIE v3	2025	2113

accessed by electron scattering. This new information will enable tests of nuclear models heretofore based solely on electron scattering [75,76].

Table I provides the χ^2 for model predictions of the $p_{\perp} - p_{\parallel}$ differential cross section measurement. The models differ in additional effects added to the default version of the GENIE generator. The variations denoted “+RPA” include the Valencia RPA model [26,63], while “+2p2h” adds the Valencia prediction for the multinucleon scattering [64–66]. “+MINOS (MINERvA) π low- Q_{QE}^2 sup.” refers to an empirical resonant pion low- Q_{QE}^2 suppression based on MINOS [18] (MINERvA [73]) data. “ π tune” refers to a 57% reduction nonresonant pion production motivated by deuterium data [68].

In general, the χ^2 values for all of the models are poor, but the models with the smallest χ^2 are those that include RPA but not $2p2h$. This is in contrast to previous MINERvA measurements [54] of this channel in the lower-energy NuMI tune, indicating that the expanded phase space of this dataset is illuminating regions of mismodeling that could not be seen in prior measurements. A χ^2 table for model predictions of the single-differential cross section versus Q_{QE}^2 is available in the Supplemental Material [69].

This result is the first CCQE-like measurement at Q_{QE}^2 above 4 GeV² and spans almost 4 orders of magnitude in Q^2 . The data in this high- Q^2 region diverge from most predictions that are based on generators used by current oscillation experiments, and there are no models that are even in approximate agreement over all ranges of Q^2 . The high-statistics, double-differential cross sections will be an important benchmark for model developers who tune models for future neutrino oscillation measurements.

This manuscript was co-authored by members of the MINERvA Collaboration using the resources of the Fermi National Accelerator Laboratory (Fermilab), a U. S. Department of Energy, Office of Science, HEP User Facility. Fermilab is managed by Fermi Research Alliance, LLC (FRA), acting under Contract No. DE-AC02-07CH11359. These resources included support for the MINERvA construction project, and support for construction also was granted by the U.S. National Science Foundation under Grant No. PHY-0619727 and by the University of Rochester. Support for participating scientists was provided by NSF and DOE (U.S.), by CAPES and CNPq (Brazil), by CoNaCyT (Mexico), by Proyecto Basal FB 0821, CONICYT PIA ACT1413, Fondecyt 3170845, and 11130133 (Chile), by CONCYTEC, DGI-PUCP, and IDI/IGI-UNI (Peru), and by the Latin American Center for Physics (CLAF). We thank the MINOS Collaboration for use of its near detector data. Finally, we thank the staff of Fermilab for support of the beam line, the detector, and computing infrastructure.

*Present address: Brookhaven National Laboratory, Upton, New York 11973, USA.

- [1] K. Abe *et al.* (T2K Collaboration), *Phys. Rev. Lett.* **121**, 171802 (2018).
- [2] K. Abe *et al.* (T2K Collaboration), *Phys. Rev. D* **96**, 092006 (2017); **98**, 019902(E) (2018).
- [3] M. A. Acero *et al.* (NOvA Collaboration), *Phys. Rev. Lett.* **123**, 151803 (2019).
- [4] M. A. Acero *et al.* (NOvA Collaboration), *Phys. Rev. D* **98**, 032012 (2018).
- [5] R. Acciarri *et al.* (DUNE Collaboration), arXiv:1512.06148.
- [6] K. Abe *et al.* (Hyper-Kamiokande Proto-Collaboration), *Prog. Theor. Exp. Phys.* **2015**, 053C02 (2015).
- [7] L. Alvarez-Ruso *et al.*, *Prog. Part. Nucl. Phys.* **100**, 1 (2018).
- [8] C. H. Llewellyn Smith, *Phys. Rep.* **3**, 261 (1972).
- [9] R. Bradford, A. Bodek, H. S. Budd, and J. Arrington, *Nucl. Phys. B, Proc. Suppl.* **159**, 127 (2006).
- [10] D. H. Wilkinson, *Nucl. Phys.* **A377**, 474 (1982).
- [11] B. Maerkisch and H. Abele, arXiv:1410.4220.
- [12] K. L. Miller *et al.*, *Phys. Rev. D* **26**, 537 (1982).
- [13] T. Kitagaki *et al.*, *Phys. Rev. D* **42**, 1331 (1990).
- [14] T. Kitagaki *et al.*, *Phys. Rev. D* **28**, 436 (1983).
- [15] D. Allasia *et al.*, *Nucl. Phys.* **B343**, 285 (1990).
- [16] A. A. Aguilar-Arevalo *et al.* (MiniBooNE Collaboration), *Nucl. Instrum. Methods Phys. Res., Sect. A* **599**, 28 (2009).
- [17] K. Abe *et al.* (T2K Collaboration), *Nucl. Instrum. Methods Phys. Res., Sect. A* **659**, 106 (2011).
- [18] P. Adamson *et al.* (MINOS Collaboration), *Phys. Rev. D* **91**, 012005 (2015).
- [19] C. Adams *et al.* (MicroBooNE Collaboration), *Phys. Rev. D* **99**, 091102 (2019).
- [20] R. Smith and E. Moniz, *Nucl. Phys.* **B43**, 605 (1972).
- [21] G. A. Fiorentini *et al.* (MINERvA Collaboration), *Phys. Rev. Lett.* **111**, 022502 (2013).
- [22] K. Abe *et al.* (T2K Collaboration), *Phys. Rev. D* **92**, 112003 (2015).
- [23] J. W. Negele, *Phys. Rev. C* **1**, 1260 (1970).
- [24] J. A. Maruhn, P.-G. Reinhard, and E. Suraud, *Simple Models of Many-Fermion Systems* (Springer-Verlag, Berlin, 2009).
- [25] R. Cenni, T. W. Donnelly, and A. Molinari, *Phys. Rev. C* **56**, 276 (1997).
- [26] J. Nieves, J. E. Amaro, and M. Valverde, *Phys. Rev. C* **70**, 055503 (2004); **72**, 019902(E) (2005).
- [27] M. Martini, M. Ericson, G. Chanfray, and J. Marteau, *Phys. Rev. C* **80**, 065501 (2009).
- [28] K. M. Graczyk and J. T. Sobczyk, *Eur. Phys. J. C* **31**, 177 (2003).
- [29] S. K. Singh and E. Oset, *Nucl. Phys.* **A542**, 587 (1992).
- [30] M. Martini, N. Jachowicz, M. Ericson, V. Pandey, T. Van Cuyck, and N. Van Dessel, *Phys. Rev. C* **94**, 015501 (2016).
- [31] J. Nieves and J. E. Sobczyk, *Ann. Phys. (Amsterdam)* **383**, 455 (2017).
- [32] O. Benhar, D. Day, and I. Sick, arXiv:nucl-ex/0603032.
- [33] O. Benhar, D. Day, and I. Sick, *Rev. Mod. Phys.* **80**, 189 (2008).
- [34] D. Zeller, PhD thesis, Report No. DESY-F23-73-2, <http://inspirehep.net/record/80440>.
- [35] P. Barreau *et al.*, *Nucl. Phys.* **A402**, 515 (1983).
- [36] J. S. O'Connell *et al.*, *Phys. Rev. C* **35**, 1063 (1987).
- [37] D. S. Bagdasaryan *et al.*, Report No. YERPHI-1077-40-88, <https://faculty.virginia.edu/qes-archive/>.
- [38] R. M. Sealock *et al.*, *Phys. Rev. Lett.* **62**, 1350 (1989).
- [39] J. Nieves, I. R. Simo, and M. J. V. Vacas, *Phys. Rev. C* **83**, 045501 (2011).
- [40] G. D. Megias, J. E. Amaro, M. B. Barbaro, J. A. Caballero, T. W. Donnelly, and I. R. Simo, *Phys. Rev. D* **94**, 093004 (2016).
- [41] T. Van Cuyck, N. Jachowicz, R. González-Jiménez, J. Ryckebusch, and N. Van Dessel, *Phys. Rev. C* **95**, 054611 (2017).
- [42] R. Gran *et al.* (K2K Collaboration), *Phys. Rev. D* **74**, 052002 (2006).
- [43] V. Lyubushkin *et al.* (NOMAD Collaboration), *Eur. Phys. J. C* **63**, 355 (2009).
- [44] A. A. Aguilar-Arevalo *et al.* (MiniBooNE Collaboration), *Phys. Rev. D* **88**, 032001 (2013).
- [45] L. Fields *et al.* (MINERvA Collaboration), *Phys. Rev. Lett.* **111**, 022501 (2013).
- [46] T. Walton *et al.* (MINERvA Collaboration), *Phys. Rev. D* **91**, 071301 (2015).
- [47] J. Wolcott *et al.* (MINERvA Collaboration), *Phys. Rev. Lett.* **116**, 081802 (2016).
- [48] M. Betancourt *et al.* (MINERvA Collaboration), *Phys. Rev. Lett.* **119**, 082001 (2017).
- [49] R. Acciarri *et al.* (ArgoNeuT Collaboration), *Phys. Rev. D* **90**, 012008 (2014).
- [50] K. Abe *et al.* (T2K Collaboration), *Phys. Rev. D* **91**, 112002 (2015).
- [51] K. Abe *et al.* (T2K Collaboration), *Phys. Rev. D* **93**, 112012 (2016).
- [52] C. E. Patrick *et al.* (MINERvA Collaboration), *Phys. Rev. D* **97**, 052002 (2018).
- [53] K. Abe *et al.* (T2K Collaboration), *Phys. Rev. D* **98**, 032003 (2018).

- [54] D. Ruterbories *et al.* (MINERVA Collaboration), *Phys. Rev. D* **99**, 012004 (2019).
- [55] P. Adamson *et al.*, *Nucl. Instrum. Methods Phys. Res., Sect. A* **806**, 279 (2016).
- [56] S. Agostinelli *et al.* (Geant4 Collaboration), *Nucl. Instrum. Methods Phys. Res., Sect. A* **506**, 250 (2003).
- [57] J. Allison *et al.*, *IEEE Trans. Nucl. Sci.* **53**, 270 (2006).
- [58] L. Aliaga *et al.* (MINERVA Collaboration), *Phys. Rev. D* **94**, 092005 (2016); **95**, 039903(E) (2017).
- [59] E. Valencia *et al.* (MINERVA Collaboration), *Phys. Rev. D* **100**, 092001 (2019).
- [60] L. Aliaga *et al.* (MINERVA Collaboration), *Nucl. Instrum. Methods Phys. Res., Sect. A* **743**, 130 (2014).
- [61] D. G. Michael *et al.* (MINOS Collaboration), *Nucl. Instrum. Methods Phys. Res., Sect. A* **596**, 190 (2008).
- [62] C. Andreopoulos *et al.*, *Nucl. Instrum. Methods Phys. Res., Sect. A* **614**, 87 (2010).
- [63] R. Gran, [arXiv:1705.02932](https://arxiv.org/abs/1705.02932).
- [64] J. Nieves, I. R. Simo, and M. J. V. Vacas, *Phys. Rev. C* **83**, 045501 (2011).
- [65] R. Gran, J. Nieves, F. Sanchez, and M. J. V. Vacas, *Phys. Rev. D* **88**, 113007 (2013).
- [66] J. Schwehr, D. Cherdack, and R. Gran, [arXiv:1601.02038](https://arxiv.org/abs/1601.02038).
- [67] P. A. Rodrigues *et al.* (MINERVA Collaboration), *Phys. Rev. Lett.* **116**, 071802 (2016); **121**, 209902(E) (2018).
- [68] P. Rodrigues, C. Wilkinson, and K. McFarland, *Eur. Phys. J. C* **76**, 474 (2016).
- [69] See Supplemental Material at <http://link.aps.org/supplemental/10.1103/PhysRevLett.124.121801> for additional plots related to the muon energy scale correction, background fits, and systematic uncertainties, as well as a chi-square table for the single differential $d\sigma/dQ^2$ result
- [70] G. D'Agostini, *Nucl. Instrum. Methods Phys. Res., Sect. A* **362**, 487 (1995).
- [71] G. D'Agostini, [arXiv:1010.0632](https://arxiv.org/abs/1010.0632).
- [72] T. Auye, *Proceedings of the PHYSTAT 2011 Workshop, CERN, Geneva* (2011).
- [73] P. Stowell *et al.* (MINERVA Collaboration), *Phys. Rev. D* **100**, 072005 (2019).
- [74] A. J. R. Puckett *et al.*, *Phys. Rev. C* **85**, 045203 (2012).
- [75] A. S. Meyer, M. Betancourt, R. Gran, and R. J. Hill, *Phys. Rev. D* **93**, 113015 (2016).
- [76] I. A. Qattan, J. Arrington, and A. Alsaad, *Phys. Rev. C* **91**, 065203 (2015).